Retardation effects on plasma waves in graphene, topological insulators and quantum wires

Hai-Yao Deng[1,2] and Katsunori Wakabayashi[1,2*]
[1]*International Center for Materials Nanoarchitechtonics (WPI-MANA), National Institute for Materials Science (NIMS), Namiki 1-1, Tsukuba 305-0044, Japan and*
[2]*Department of Nanotechnology for Sustainable Energy, School of Science and Technology, Kwansei Gakuin University, Gakuen 2-1, Sanda 669-1337, Japan*
(Dated: Jan. 06, 2015)

Retardation effects (REs) are known to cause a crossover from linear to sublinear behaviors in the dispersion relation of two-dimensional (2D) plasma waves at long wave lengths. In the present work, we systematically analyze REs on plasma waves in both 2D and one-dimensional (1D) electron gases and clarify the experimental conditions for observing the crossover. We show that graphene is the only material that might gratify the conditions with current technology. Although it closely imitates graphene, the surface of three-dimensional (3D) topological insulators is found not suitable for this purpose due to strong electronic scattering by intrinsic disorder. We also show that the crossover, though theoretically possible, virtually never occur in 1D plasma. In addition, the relevance of our results to teraherz plasmonics is discussed.

I. INTRODUCTION

Electrons in solids can undergo plasma oscillations due to long-range Coulomb forces. The fundamental plasma theory was accomplished long ago.[1] In three dimension (3D), plasma frequency is nearly independent of the wave number q.[2] However, in two dimension (2D) it possesses a sublinear dispersion relation,[3–6] $\omega_p^{2D} \sim \sqrt{q}$, which would derive unphysical superluminal transmission of wave packets at sufficiently small $q \sim q^*$, viz. the group velocity $v_g^{2D} = \partial_q \omega_p^{2D} \sim 1/\sqrt{q}$ would exceed the speed of light c.[7] Retardation effects (REs, resulting from the finite speed of light) critically modify the dispersion and eventually the dispersion becomes linear,[7] $\omega_p^{2D} \sim cq$ for $q \ll q^*$. Experimentally studying the crossover around q^* turns out to be difficult, partly because q^* is typically minuscule. Simple estimate shows that $q^* \sim 1\ \mathrm{Km}^{-1}$ for 2D electron gas precipitated on the surface of liquid helium (electron density $n_0 \sim 10^7 \mathrm{cm}^{-2}$) or $q^* \sim 1\ \mathrm{dm}^{-1}$ for that formed in semiconductor heterostructures ($n_0 \sim 10^{11}\mathrm{cm}^{-2}$). Therefore, q^{*-1} is generally in excess of available sample dimensions. The crossover phenomenon has thence not been thoroughly analyzed in existing studies.

The interest in 2D plasma has recently been boosted by the advent of graphene,[8,9] which is an atomically thin sheet of carbon atoms, and 3D topological insulators (TIs) that harbor gapless energy bands on their surfaces.[10,11] These materials have one common feature in their electronic structure:[12,13] near the Fermi level ε_F their charge carriers behave as 2D massless Dirac fermions characterized by conical energy-momentum dispersion, $\varepsilon(\vec{p}) = v_F p$. Here $v_F \approx 10^6 \mathrm{ms}^{-1}$ denotes the Fermi velocity and $p = |\vec{p}|$ with $\vec{p}$ being the momentum. This feature makes them very attractive for applications in surface plasmonics, which is poised as a viable path toward nanophotonics and terahertz (THZ) technology.[14–16] In the latter, 2D plasma has been gaining a progressively significant status as it might provide a means of attaining efficient coupling with THZ electromagnetic waves and thereby an avenue to manipulate them. Due to a fundamental mismatch between the wavelength of THZ waves and that of plasma at the same frequency, such coupling is generically weak and plasmonic crystals are required to enhance it.[17] However, if it is engineered into the regime where $q < q^*$, the plasma will have the same dispersion relation as electromagnetic waves and are expected to show strong light-matter interaction.[18] Therefore, the wavelength mismatch can be mitigated and the need for artificial structuring may be largely dispensed with.

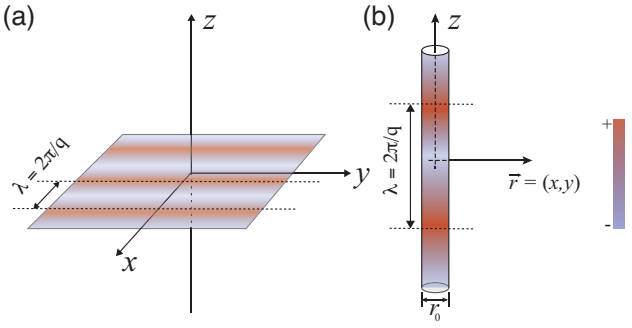


FIG. 1. (a) A sheet of electron gas is placed in the $x-y$ plane, in which plasma waves are incited to propagate along x direction. (b) Sketch of a quantum wire with lateral dimension $\sim r_0$. Plasma waves are propagating along the wire (z direction). Throughout the paper, we use $\vec{x} = (x, y, z)$ and reserve $\vec{r} = (x, y)$ for points in the $x-y$ plane. Colors schematically encode charge density.

In this paper we study REs on plasma in graphene, TIs and quantum wires such as graphene nanoribbons (GNRs). Unlike previous work,[18,19] we systematically clarify the crossover scenario by two parameters q^* and $\omega^* = cq^*$. Their dependence on the electronic structure is then established. Practical requirements for observing the crossover are clarified. We find that in order to observe the crossover, not only the sample dimension must be sufficiently bigger than q^{*-1} but also sufficiently clean so that the electronic scattering rate τ^{-1} is much lower than ω^*. Checking the conditions against common 2D electron gases, we find graphene to be the only system that might meet both conditions. Although a TI surface closely imitates graphene, the small bulk band gap (~ 0.3eV) and the relatively strong electronic scattering due to intrinsic disorder makes it inferior. Moreover, we show that REs are negligibly small in realistic quantum wires and can thence be

ignored under ambient circumstances. Estimate shows that high-quality and large-area graphene might be used for detecting THZ waves.

In the next section, we present the framework and derive the generic expressions for 2D. Similar results for one-dimension (1D) systems are given in Appendix A. The REs-driven crossover phenomenon in graphene, TI and quantum wires are scrutinized in detail in Sec. III, where effects due to the presence of dielectrics are also briefly discussed. In Sec. IV, we analyze electronic scattering effects on observing the crossover. We discuss our results and conclude the paper in Sec. V.

II. FORMALISM

Plasma are self-sustained long wavelength charge density waves. To establish the equation of motions for the charge density (assuming neutrality on the whole), which we designate by $n(\vec{x},t)$, let us begin with the continuity equation

$$\partial_t n(\vec{x},t) + \partial_{\vec{x}}\cdot \vec{j}(\vec{x},t) = 0, \tag{1}$$

which locally embodies the conservation of total charge entailed by gauge symmetry. Here $\vec{j}(\vec{x},t)$ stands for the electrical current density while $\vec{x} = (x,y,z)$ represents a point in space and t an instant in time. Next we relate $\vec{j}(\vec{x},t)$ to local fields via an appropriate response function. For our purpose, we only consider weak electric fields $\vec{E}(\vec{x},t)$. In the linear response regime we can write

$$j^i(\vec{x},t) = \sum_j \int d\vec{x'} \int dt'\, \sigma_0^{ij}(\vec{x},\vec{x'},t-t')\, E^j(\vec{x'},t'), \tag{2}$$

where the indice are $i,j = x,y,z$ and σ_0 denotes the conductivity tensor of the system without taking into account electromagnetic interactions. In addition, according to Maxwell's theory we cast

$$\vec{E}(\vec{x},t) = -\partial_{\vec{x}}V(\vec{x},t) - \frac{1}{c}\partial_t \vec{A}(\vec{x},t), \tag{3}$$

where $V(\vec{x},t)$ and $\vec{A}(\vec{x},t)$ represent the scalar and vector potential fields, respectively. $c \approx 3\times 10^8 \mathrm{ms}^{-1}$ is the speed of light in vacuum. In the Lorenz gauge the Fourier components of $V(\vec{x},t)$, $\vec{A}(\vec{x},t)$, $n(\vec{x},t)$ and $\vec{j}(\vec{x},t)$, denoted by $V_\omega(\vec{x})$, $\vec{A}_\omega(\vec{x})$, $n_\omega(\vec{x})$ and $\vec{j}_\omega(\vec{x})$ respectively, satisfy the following equations[20]

$$\left(\partial_{\vec{x}}^2 + \frac{\omega^2}{c^2}\right)\begin{pmatrix} V_\omega(\vec{x}) \\ \vec{A}_\omega(\vec{x})\end{pmatrix} = -4\pi \begin{pmatrix} n_\omega(\vec{x}) \\ c^{-1}\vec{j}_\omega(\vec{x})\end{pmatrix}. \tag{4}$$

Equations (1) - (4) complete the semi-classical (i.e., treating the electromagnetic fields classically) description of plasma waves. They only involve quantites that exist irrespective of the underlying microscopic dynamics. The bare conductivity tensor σ_0^{ij} serves as the single input, which can be either calculated or just phenomenological. This description reduces to the random phase approximation (RPA)[1,4,21] in the static limit $c\to\infty$.[22] Or it boils downs to the hydrodynamical approach[7,23,24] if one assumes a Drude-Boltzmann model[25] for σ_0^{ij}. Hitherto we have not included any dielectrics in the equations. Their effects will be briefly discussed in Sec.III.

Throughout this paper we confine ourselves to long wavelength responses (which is relevant for plasma) of isotropic systems, so that σ_0 becomes a local scalar, viz.

$$\sigma_0^{ij}(\vec{x},\vec{x'},\tau) = \sigma_0(\tau)\,\delta_{ij}\,\delta(\vec{x}-\vec{x'}). \tag{5}$$

Here $\sigma_0(\tau)$ (together with its Fourier transform σ_0^ω) will be specified in later sections.

Let us apply those equations to a homogeneous 2D system lying in the plane $z=0$ as depicted in Fig. 1 (a). We seek plane wave solutions for $n(\vec{x},t)$ and $\vec{j}(\vec{x},t)$. Without loss of generality we may put the wave vector as $\vec{q} = (q,0)$, thereby decoupling j^y from both j^x and n. Then it suffices to consider $\vec{j} = (j,0)$, i.e. $j^y \equiv 0$ and hence $A^y = 0$ by Eq. (4) so that $\vec{A} = (A,0)$. Accordingly, we write

$$s(\vec{x},t) = s_{q\omega}\, e^{i(qx-\omega t)}\,\delta(z), \quad s = n,\, j/c. \tag{6}$$

From the continuity equation (1) we infer that

$$j_{q\omega} = (\omega/q)\, n_{q\omega}. \tag{7}$$

The linearity of Eq. (4) dictates that $\psi_\omega(\vec{x}) = \psi_{q\omega}(z)\, e^{i(qx-\omega t)}$, where $\psi = V, A$. Using (4) we get

$$\left(\kappa^2 - \partial_z^2\right)\,\psi_{q\omega}(z) = 4\pi s_{q\omega}\,\delta(z), \tag{8}$$

where $\kappa^2 = q^2 - \frac{\omega^2}{c^2}$. Solving this equation and using (7) we arrive

$$\begin{pmatrix} V_{q\omega}(z) \\ A_{q\omega}(z)\end{pmatrix} = 2\pi \begin{pmatrix} 1 \\ \frac{\omega}{cq}\end{pmatrix} n_{q\omega}\, e^{-\kappa|z|}\,\kappa^{-1}. \tag{9}$$

We require κ to be real positive, $\kappa = \sqrt{q^2-\omega^2c^{-2}}$ with $qc > \omega$, so that no radiation emanates from the plasma. Combining Eqs. (3) and (9), we see that the y-component of the local electric field vanishes. At $z=0$ the x-component, denoted by $E(\vec{r},t)$, is given by

$$E(x,y,t) = E_{q\omega}\, e^{i(qx-\omega t)}, \quad E_{q\omega} = \frac{\kappa^2}{iq}\, V_{q\omega} = \frac{2\pi}{i}\,\frac{\kappa}{q}\, n_{q\omega}, \tag{10}$$

which together with (2) and (5) yields

$$j_{q\omega} = \sigma_0^\omega\, E_{q\omega} = \frac{2\pi}{i}\,\frac{\kappa}{q}\,\sigma_0^\omega\, n_{q\omega}, \tag{11}$$

Equating (11) with (7) leads to

$$\omega + 2\pi i\,\kappa\,\sigma_0^\omega = 0, \tag{12}$$

which will be used to determine the dispersion relation $\omega_p^{2D}(q)$ for 2D plasma.

We can derive a similar equation as (12) for determining the dispersion relation of plasma waves in quantum wires sketched in Fig. 1 (b). Referring the calculation details to Appendix A, here we only quote the result. Let the wave with wave number q propagate along a wire of radius r_0. Then the desired equation reads

$$\omega + 2i\sigma_0^\omega \kappa^2 K_0(\kappa r_0) = 0, \tag{13}$$

where $K_0(z)$ is the modified Bessel function.

TABLE I. Expressions for the factor F involved in the Drude-Boltzmann conductivity, $\sigma_0^\omega = i\frac{F}{\omega}$ (dissipationless limit). We use $\varepsilon(p)$ to denote the energy-momentum relation of the system under question, n_0 is the average electron density, m the effective mass, v_F the Fermi velocity, ε_F the Fermi level, $N(\varepsilon)$ density of states per unit area, e the elementary charge and $\hbar$ ($h = 2\pi\hbar$) the reduced Planck constant.

$\varepsilon(p)$	Parabolic (2D)	Linear (2D)	Parabolic (1D)	Linear (1D)
F	$\frac{n_0 e^2}{m}$	$\frac{e^2 v_F^2 N(\varepsilon_F)}{2}$	$\frac{n_0 e^2}{m}$	$\frac{e^2 v_F}{h}$

III. CHARACTERIZING THE CROSSOVER

Anticipating that REs become pronounced only at very small q and ω, we may assume the Drude-Boltzmann model for the bare conductivity. Namely, we put

$$\sigma_0^\omega = \frac{F\tau}{1 - i\omega\tau}, \tag{14}$$

where F is a prefactor that depends on the particulars of the system (see Table I) and τ is the transport relaxation time.[25]

For 2D systems, it is convenient to express ω and τ^{-1} in units of $\omega^* = 2\pi F/c$ and q of $q^* = \omega^*/c$. Then we can rewrite Eq. (12) as follows

$$\omega + i\sqrt{q^2 - \omega^2}\,\frac{\tau}{1 - i\omega\tau} = 0, \tag{15}$$

which depends on a single parameter τ. Its solution $\Omega_p^{2D} = \omega_p^{2D} - i\gamma_p^{2D}/2$ gives the plasma frequency ω_p^{2D} and the damping rate γ_p^{2D}. In the limit $\tau \to \infty$, γ_p^{2D} vanishes and ω_p^{2D} is given by (after recovering the units)

$$\omega_p^{2D} = \omega^* \sqrt{\frac{1}{2}\left\{\sqrt{1 + 4\left(\frac{q}{q^*}\right)^2} - 1\right\}}, \quad \text{for } \tau \to \infty, \tag{16}$$

Finite but large τ will make negative corrections of the order τ^{-2} to ω_p^{2D}. There is a crossover to occur around q^*. Actually, we find

$$\omega_p^{2D} \approx \begin{cases} \omega^*\sqrt{q/q^*}, & \text{if } q \gg q^*, \\ \omega^*\,(q/q^*) = cq, & \text{if } q \ll q^*. \end{cases} \tag{17}$$

The associated v_g goes as $q^{-1/2}$ for large q but saturates at c for small q. The crossover is clear in Fig. 2, where ω_p^{2D} is plotted versus q.

The value of q^* varies significantly from one system to another. For systems with quadratic energy-momentum relation, $\varepsilon(\vec{p}) = \frac{\vec{p}^2}{2m}$, where m denotes the effective electronic mass, we have $F = \frac{n_0 e^2}{m}$ with n_0 being the average electron density. Expressing $n_0 = n_0^* \times 10^{16}\mathrm{cm}^{-2}$ and $m = m^* \times 9.1 \times 10^{-31}\mathrm{Kg}$, we obtain

$$\omega^* = \frac{2\pi n_0 e^2}{mc} \approx \frac{n_0^*}{2m^*} \times 10^{15}\mathrm{Hz}, \quad q^* \approx \frac{n_0^*}{6m^*} \times 10^7\mathrm{m}^{-1}. \tag{18}$$

For electrons precipitated on the surface of liquid helium, on which the 2D plasma dispersion [upper line in Eq. (17)] was first verified[5,26], one has $n_0^* \sim 10^{-9}$ and $m^* \sim 1$. Thus, $\omega^* \sim 0.5\mathrm{MHz}$ and $q^* \sim 2\mathrm{Km}^{-1}$, which is too small a value to be experimentally achieved. To observe the crossover, a sample area much larger than $q^{*-2} \sim 0.25\mathrm{km}^2$ is demanded. For electrons accumulated at the interface of a semiconductor heterojunction like AlGaAs/GaAs, typically $n_0^* \sim 10^{-5}$ and $m^* \sim 0.1$.[27] Therefore, $\omega^* \sim 50\mathrm{GHz}$ and $q^* \sim 1.67\mathrm{cm}^{-1}$, which are still very tiny for realization. The sample area required far surpasses $2.78\mathrm{dm}^2$. These numerics show that REs are generically negligible in conventional 2D electron gases.

We proceed to reason that graphene has a disparate story. This material in its pristine form has a conduction and a valence band near the Fermi level ε_F, which touch conically at the corners of the first Brillouin zone.[28,29] Relative to the neutrality point (chosen to be $\varepsilon = 0$), the electronic energy-momentum relation is nearly linear: $\varepsilon(\vec{p}) = v_F|\vec{p}|$, where $v_F \approx 10^6\mathrm{ms}^{-1}$. For ε_F close to the neutrality point, interband transitions prevail at all frequencies and hence Drude-Boltzmann theory [Eq. (14)] is not applicable. Nevertheless, far away from that point interband transitions are greatly suppressed at frequencies below $2\varepsilon_F/\hbar$. Under such circumstances, we may still use Eq. (14). As shown in Ref.[30], for graphene $F = e^2 v_F^2 N(\varepsilon_F)/2$, where $N(\varepsilon_F) = \frac{\sqrt{\pi n_0}}{h v_F}$ denotes the density of states per unit area per valley per spin. Now we find

$$\omega^* = \frac{\pi e^2 v_F^2 N(\varepsilon_F)}{c} \approx \sqrt{n_0^*} \times 6.5 \times 10^{13}\mathrm{Hz},$$
$$q^* \approx \sqrt{n_0^*} \times 2.1 \times 10^5\mathrm{m}^{-1}. \tag{19}$$

Current doping technology can commonly achieve $n_0^* \sim 10^{-4}$ in graphene,[31] for which $\omega^* \sim 0.65\mathrm{THz}$ and $q^* \sim 2.1\mathrm{mm}^{-1}$. Good quality single crystal monolayer graphene sheet of sizes $\sim 1\mathrm{cm}^2$ can hopefully be fabricated using chemical vapor deposition method.[32] Therefore, observation of the REs-driven crossover is fairly plausible in graphene.

To complete the analysis, let us examine TIs, which have recently caused a great sensation. TIs possess surfaces which each features a pair of conically dispersing energy bands crossing Fermi level, in close analogy with graphene.[11] The same $\varepsilon(\vec{p})$ applies here as for graphene, but with $v_F \sim 6 \times 10^5\mathrm{ms}^{-1}$. The lacking of valley and spin degeneracy leads to $N(\varepsilon_F) = \frac{\sqrt{\pi n_0}}{2\hbar v_F}$. As a result, $q^* \sim \sqrt{n_0^*} \times 5 \times 10^4\mathrm{m}^{-1}$ becomes much smaller. Additionally, There is an upper bound on n_0^* because of the existence of the bulk bandgap, which is $\sim 0.3\mathrm{eV}$ for Bi_2Se_3, the most extensively studied TI. The Fermi level must be well inside this gap to avoid strong mixing with bulk bands. Namely, $\varepsilon_F = \hbar v_F \sqrt{4\pi n_0} \approx 10\sqrt{n_0^*}\mathrm{eV} < 0.1\mathrm{eV}$, which gives $n_0^* < 10^{-4}$. This fixes $q^* < 0.5\mathrm{mm}^{-1}$, corresponding to a surface area no less than $10\mathrm{mm}^2$. The observed carrier mobility in TIs is much lower than that in graphene, due to intrinsic dopant disorder.[33,34] This means relatively smaller τ and hence stronger plasma damping, which makes low frequency (relevant to REs) observation especially difficult (see the next section). Moreover, the fabrication of good quality TIs with desired surface area is currently formiddable. The coupling

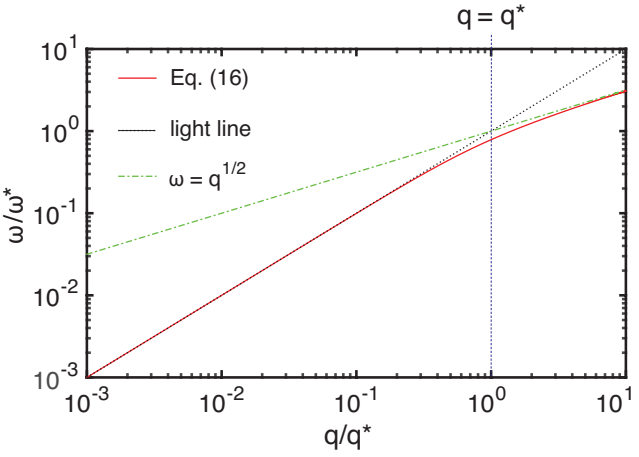


FIG. 2. 2D plasma dispersion relation $\omega_p^{2D}(q)$. The red solid curve is given by Eq. (16), which reduces to the green solid curve for $q > q^*$ but becomes degenerate with the light line (dashed curve) for $q < q^*$. The crossover is controlled by the single parameter q^*, which varies significantly from one system to another. In units of $\omega^* = cq^*$ and q^*, ω_p^{2D} assumes a form that is regardless of the materials.

between parallel surfaces is likely to erase the crossover phenomenon.[7]

Graphene has an additional merit that it can be inserted between dielectrics ϵ with relative ease. The main effects of the dielectrics consist of reducing c to $c/\sqrt{\epsilon(qd)}$ and subsequently increasing q^* to $\epsilon(q^*d)q^*$. Here d is the separation of graphene layer from the dielectric layer and $\epsilon(qd) = \epsilon\cosh(qd)/2$, which becomes ϵ at long wavelengths.[35] This further decreases the desired sample sizes and then lowers the barrier of observing the REs-driven crossover. For example, taking the dielectric to be HfO_2 with $\epsilon \approx 22$ and $n_0^* \sim 10^{-3}$, we expect $q^* \sim 0.12\mu\text{m}^{-1}$ and a sample area of $\sim 100\mu\text{m}^2$, which can already be obtained using current fabrication methods.[32,36] Let us also mention hexagonal boron nitride (hBN) on this occasion. Although it has a smaller $\epsilon \approx 4$, hBN is capable of preserving the high mobility of graphene.[37] As we will discuss in the next section, high mobility is also crucial in observing the crossover. We note that the surface of TIs is sandwiched between the bulk ($\epsilon \approx 100$ for Bi_2Se_3[34]) and the vacuum. This gives an effective dielectric constant of ≈ 50 and thus $q^* \leq 0.025\mu\text{m}^{-1}$.

For quantum wires, an analogous but more subtle reasoning has been presented in Appendix A, where it is shown that REs are not discernible at all. The predicted crossover occurs at $q^* \sim r_0^{-1}e^{-(c/c^*)}$, which is practically zero in the systems known to us. Here $c^* = \sqrt{2F}$, with F given in Table I.

IV. DAMPING EFFECTS

We have so far focused on the limit $\tau \to \infty$. In reality, τ is finite and the plasma spectrum can be modified. To gain some insights, let us first consider 2D plasma in the extreme that $\omega\tau \gg 1$, whereby $(\omega\tau)^{-1}$ serves as a small parameter for perturbative treatment. Let us write $\Omega_p^{2D} = \omega_p^{2D} + \delta\omega_p^{2D} - i\gamma_p^{2D}/2$, where ω_p^{2D} is prescribed by Eq. (16), and substitute it in (15). To the first order in τ^{-1}, we find $\delta\omega_p^{2D} \approx 0$ and

$$\gamma_p^{2D} \approx \frac{1}{\tau}\,\frac{1}{1+\frac{1}{2}\left(\frac{\omega^*}{\omega_p^{2D}}\right)^2} \approx \begin{cases}\tau^{-1}, & \text{if } q \gg q^*,\\ 0.7\tau^{-1}, & \text{if } q \sim q^*,\\ 0, & \text{if } q \ll q^*.\end{cases} \tag{20}$$

Note that γ_p^{2D} can be directly measured by e.g. electron energy loss spectroscopy (EELS).[1] The plasma shows up as a peak in EELS at fixed q. The width of this peak gives γ_p^{2D}. From Eq. (20), we infer that the peak will get broadened as q increases.

In the other extreme where $\omega\tau \ll 1$, plasma becomes heavily damped and we expect to see a central peak (relaxational mode) in EELS for not-so-big q. Actually, to the first order in $\omega\tau$, which is treated as a small parameter, Eq. (15) becomes

$$\omega + i\omega^*\tau\sqrt{c^2q^2 - \omega^2} \approx 0, \tag{21}$$

yielding $\omega_p^{2D} \approx 0$ and $\gamma_p^{2D} \approx 2\,\omega^*\tau\,qc$. This shows that the central peak gets narrower when q decreases. For sufficiently big q, the central peak disappears.

The overall profile of EELS can be numerically assessed. For this purpose, we resort to the fact that the l.h.s. of Eq. (12) [or equivalently (15)] corresponds to the dynamic dielectric function $\epsilon(\omega, q)$ of the electron gas. EELS is then mainly determined as $\text{Im}\left(-\frac{1}{\epsilon(\omega,q)}\right)$, which is a positive-definite function in ω. In Fig. 3 we plot it for representative values of q and τ. In line with the analytical expressions, we see that (i) the plasma dispersion is linear for $q < q^*$ but becomes sublinear for $q > q^*$; (ii) damping effects are more pronounced for higher q and (iii) for very heavy damping ($\omega^*\tau < 1$) a central peak appears for q around q^*. To unambiguously observe the crossover, it is necessary that $\omega^*\tau > 1$.

Let us compare the EELS for the 2D systems scrutinized in Sec. III. For systems with quadratic energy-momentum dispersion, we can relate τ to the electronic mobility $\mu = \mu^*\frac{\text{cm}^2}{\text{V}\cdot\text{s}}$, i.e. $\tau = (m/e)\mu$. By Eq. (18), $\omega^*\tau \approx 0.28 \times n_0^*\,\mu^*$, which does not rely on m^*. For electrons living on the surface of Helium at very low temperatures, $\mu^* \sim 10^5$ and we estimate that $\omega^*\tau \sim 0.003$, which is much smaller than unity. Hence, in the vicinity of q^*, we expect to see a central peak. The experiment performed in e.g. Ref.[5] looked at $q \gg q^*$ and the authors were able to see the dispersion of ω_p^{2D}. For electrons accomodated in high quality AlGaAs/GaAs heterojunctions, it is realistic to take $\mu^* \sim 10^7$ and then $\omega^*\tau \sim 28$. Therefore, even for $q \sim q^*$ we expect to see univocal plasma dispersion. Unfortunately, available sample sizes are still way below what is desired. For graphene, τ may be conveniently estimated using the value of electronic mean free path l_e and v_F, namely, $\tau = l_e/v_F$. By Eq. (19), this leads to $\omega^*\tau \approx 65 \times \sqrt{n_0^*} \times l_e^*$, with $l_e = l_e^*\,\mu\text{m}$. Good graphene samples possess $l_e \sim 10\mu\text{m}$, which puts $\omega^*\tau \sim 6.5$. The best TIs so far have l_e that is only a few percent of that of graphene. In this respect, graphene is

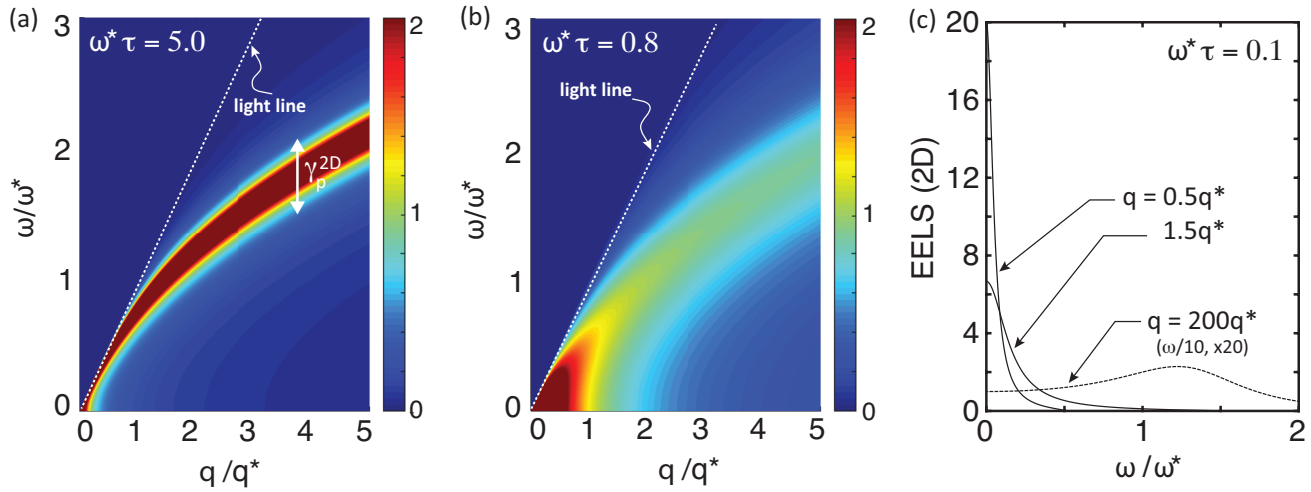


FIG. 3. Electron energy loss spectra (EELS) evaluated by Im$-\left(\epsilon^{-1}(\omega,q)\right)$, with $\epsilon(\omega,q)$ given by the left hand side of Eq. (15). EELS is useful in unveiling the effects of electronic scattering (scattering rate = τ^{-1}) on plasma dispersion $\omega_p^{2D}(q)$ and life time, which is the inverse of the broadening factor $\gamma_p^{2D}(q)$. The profile of EELS critically depends on the value of $\omega^*\tau$. As shown in panel (a), if $\omega^*\tau > 1$, the plasma disperses according to ω_p^{2D} with γ_p^{2D} increasing as q increases. However, as displayed in (b), if $\omega^*\tau < 1$, a nondispersive central peak is seen for q around q^*. In (c), we plot frequency scan for three values of q. For $q \sim q^*$ (curves with $q = 0.5q^*$ and $q = 1.5q^*$), central peaks are revealed, as in (b). For very large q (e.g. $q = 200q^*$), very weak dispersion remains. For the sake of comparison, the line labelled $q/q^* = 200$ has been multiplied by 20 and ω has been rescaled by a factor 10. To observe the crossover phenomenon, it is necessary that $\omega^*\tau > 1$.

most suitable for studying the REs-driven crossover in plasma dispersion.

Apart from EELS, optical techniques can also be used to extract the same information. For example, one may study the reflection (R) and transmission (T) of normally incident radiation on the sample. From TR^{-1}, one can infer the dielectric function $\epsilon(\omega,q)$ and then plasma properties.

V. DISCUSSIONS AND CONCLUSIONS

In summary, we have derived two criteria that must be fulfilled in order to observe the REs-driven crossover in 2D and 1D plasma dispersion relations. Firstly, the system size must be much larger than q^{*-1}. Secondly, the system must be sufficiently pure so that the electronic scattering rate is much lower than $\omega^* = cq^*$. The criteria have been systematically checked against common 2D and 1D electron gases. We synthesize the results in Table II. We found that the crossover virtually never occurs in 1D. Among 2D systems, to our knowledge the only candidate that can hopefully meet both criteria seems to be graphene.

In actual setup, we propose to sandwitch graphene between two dielectrics, so as to further increase q^* and reduce the minimum flake size. To this end, hBN may be used. Although its dielectric constant is smaller than HfO_2, hBN is able to preserve the high electronic mobility of graphene. The minimum sample area required is then estimated of $\sim 0.01\text{mm}^2$. Note that gating structure and bilayer coupling must be avoided, as it will have dramatic impact on plasma dispersion[7,23] and could erase the desired phenomenon.

Our estimate shows that the crossover frequency ω^* for typical graphene samples falls within the THZ regime, whereby the plasma dispersion follows closely that of THZ electromagnetic waves. Thus, the wavelength mismatch problem that has plagued the THZ community for years may be bypassed by optimizing graphene. The present study is expected to be useful in the design of THZ detectors.

Let us note that the use of Drude-Boltzmann formula for σ_0^ω [Eq. (14)] does not undermine our results. This is because the scenario under question occurs on the scale of q^{*-1}, which is much larger than atomic dimensions. The characteristic frequency ω^* is tiny in comparison with energy bandgap (or $2\varepsilon_F$ in case of graphene). Quantum effects play a minor role under such circumstances: the conductivity calculated via quantum mechanical perturbative theory actually reduces to Eq. (14).

Another concern pertains to coupling with optical phonons arising from the substrate supporting the 2D sample. Experiments[38] have demonstrated strong coupling around $q \sim 1\text{nm}^{-1}$ between graphene and silicon carbide substrate. However, we do not expect this coupling to be significant in the regime of $q \sim q^*$. In this regime, the phonon frequency (which is highest at $q = 0$) is much higher than that (lowest at $q = 0$) of plasmon. This frequency mismatch effectively decouples them at small q, in accord with experiments.[38]

ACKNOWLEDGMENTS

HYD acknowledges useful discussions with K. Florian. This work is supported by JSPS fellowship and KAKENHI (Project Nos. 15K13507, 25107005) from MEXT of Japan.

TABLE II. Estimated order of magnitudes of several parameters which are relevant for observing the REs-driven crossover in 2D plasma dispersion relation $\omega_p^{2D}(q)$. Four systems are listed: electrons precipitated on the surface of liquid helium, AlGaAs/GaAs heterojunction, graphene and surface of 3D topological insulators (TIs). The parameters considered are: average electron density $n_0 = n_0^* \times 10^{16}\text{cm}^{-2}$, electronic effective mass $m = m^* \times 9.1 \times 10^{-31}\text{Kg}$, $\omega^* = 2\pi F/c$ and $q^* = \omega^*/c$ as well as $\omega^*\tau$. Here $c \approx 3 \times 10^{10}\text{cm} \cdot \text{s}^{-1}$ denotes the speed of light in vacuum, F is given in Table I and τ is the electronic relaxation time. Two conditions must be gratified to observe the crossover: (i) sample dimension $\gg q^{*-1}$ and (ii) $\omega^*\tau > 1$. For graphene and TIs, m does not exist, as indicated by a hyphen in the entry.

System	Helium surface[26]	AlGaAs/GaAs[39]	Graphene[14,36,40–42]	TIs[33]
n_0^*	10^{-9}	10^{-5}	10^{-4}	10^{-4}
m^*	1	0.1	-	-
ω^*	1 MHz	10 GHz	1 THz	0.1 THz
q^*	1 Km^{-1}	1 cm^{-1}	1 mm^{-1}	0.3 mm^{-1}
$\omega^*\tau$	0.003	28	6.5	0.01 [a]

[a] For best quality graphene $\mu^* \sim 10^5$ while for best TIs $\mu^* \sim 10^3$, which underlies this value. Here $\mu = \mu^* \frac{\text{cm}^2}{\text{V}\cdot\text{s}}$ denotes electronic mobility.

Appendix A: Quantum wires

Plasma oscillations in quantum wires were optically detected over two decades ago[43,44] and have since been intensively studied.[45,46] Here we nalyze the REs-driven crossover in quasi-1D systems including graphene nanoribbons.

We imagine a homogeneous 1D system lying along the z-axis, as portrayed in Fig. 1 (b). For convenience, we shall write $\vec{r} = (x, y)$. In analogy with Eq. (6), we make the following ansatz

$$s(\vec{\imath}, t) = s_{q\omega}\, e^{i(qz-\omega t)}\, \delta^2(\vec{r}), \quad s = n, j/c. \tag{A1}$$

Here j is the z-component of $\vec{j}$. The continuity equation (7) still holds, whereas Eq. (8) is modified to be

$$\left(\kappa^2 - \partial_{\vec{r}}^2\right)\, \psi_{q\omega}(\vec{r}) = 4\pi s_{q\omega}\, \delta^2(\vec{r}), \tag{A2}$$

where we have defined $\psi(\vec{\imath}, t) = \psi_{q\omega}(\vec{r})e^{i(qz-\omega t)}$ with $\psi = V, A$. Here A denotes the z-component of $\vec{A}$. $\kappa = \sqrt{q^2 - \omega^2/c^2}$ remains the same as before. The solution to Eq. (A2) is given by

$$\psi_{q\omega}(\vec{r}) = 2\, K_0(\kappa r)\, s_{q\omega}, \tag{A3}$$

where $r = \left|\vec{r}\right|$ and $K_0(z)$ denotes the zeroth order modified Bessel function of second kind. Again $A_{q\omega}(\vec{r}) = (\omega/qc)V_{q\omega}(\vec{r})$. The z-component of the local electric field is obtained as follows

$$E(\vec{\imath}, t) = E_{q\omega}(\vec{r})\, e^{i(qz-\omega t)}, \quad E_{q\omega}(\vec{r}) = 2\, \frac{\kappa^2}{iq}\, K_0(\kappa r)\, n_{q\omega}. \tag{A4}$$

The limit $r \to 0$ is ill-defined for $E_{q\omega}(\vec{r})$. Instead of $r \to 0$, we shall take $r = r_0$, where r_0 signifies the fact that in reality any 1D system has a lateral dimention of order $r_0 \sim 10^{-10}\text{m}$. [47] Henceforth, from Eqs. (2) and (5) we have

$$j_{q\omega} = 2\sigma_0^\omega\, \frac{\kappa^2}{iq}\, K_0(\kappa r_0)\, n_{q\omega} = \frac{\omega}{q}\, n_{q\omega}, \tag{A5}$$

where the second equality comes from the continuity equation. Finally we obtain

$$\omega + 2i\, \sigma_0^\omega\, \kappa^2\, K_0(\kappa r_0) = 0. \tag{A6}$$

This equation determines the dispersion relation $\omega_p^{1D}(q)$ for 1D plasma.

The bare conductivity is given by Eq. (14), where the factor F is to be specified later. Introducing $Q = \frac{\omega}{c}$ and expressing all wave numbers (including both q and Q) in units of r_0^{-1}, we can recast Eq. (A6) in the following form (neglecting damping effects, viz. $\tau \to \infty$)

$$\left(q^2 - Q^2\right)\, K_0\left(\sqrt{q^2 - Q^2}\right) = \lambda\, Q^2,\ \lambda = \left(\frac{c}{c^*}\right)^2,\ c^* = \sqrt{2F}, \tag{A7}$$

which depends on a single parameter λ. The static limit has $c \to \infty$ and hence $\lambda \to \infty$, where Q is of the order $\lambda^{-1/2}$. In case $q \gg Q$, one can drop the Q^2 on the l.h.s. in (A7) to get $Q \approx (c^*/c)\ q\ \sqrt{K_0(q)}$, which would produce a singular group velocity $v_g \approx c^* \sqrt{K_0(q)}$ at small q. On other hand, for q lying close to zero, we may make the ansatz that $Q \approx V_g\, q$, where $V_g = v_g/c$ can be analytically evaluated. Approximating $K_0(z) \approx \ln(2/z) - \gamma$ (here $\gamma \approx 0.577$ denotes the Euler constant) and differetiating Eq. (A7), we find

$$2\lambda Q V_g + q\, \left(1 + \ln(q^2 - Q^2)\right) = 0. \tag{A8}$$

Now using (A7) to rewrite $\ln(q^2 - Q^2) \approx \frac{2\lambda Q^2}{Q^2 - q^2}$ and plugging it in this equation, we obtain $2\lambda V_g^2 + V_g^2 - 1 = 0$, which yields

$$V_g = \sqrt{\frac{\sqrt{1 + 8\lambda} - 1}{4\lambda}} \approx \begin{cases} 1, & \text{if } \lambda \ll 1, \\ (2\lambda)^{-\frac{1}{4}}, & \text{if } \lambda \gg 1. \end{cases} \tag{A9}$$

As required, $V_g < 1$ always. Piecing everything together, we see that there must exist a crossover to occur around some wave number q^*, above which $v_g/c \sim (c^*/c)\sqrt{\ln q^{-1}}$ while below it $v_g/c \sim V_g$. Obviously, we have $(c^*/c)\sqrt{\ln q^{*-1}} \sim V_g$. After recovering the units, it gives

$$q^* \sim r_0^{-1}\, e^{-\left(\frac{V_g c}{c^*}\right)^2} \approx r_0^{-1}\, e^{-\,0.71\,\times\,\sqrt{\lambda}}, \tag{A10}$$

where the second equality follows from the fact that λ generally far exceeds unity. Now we see that 1D plasma dispersion

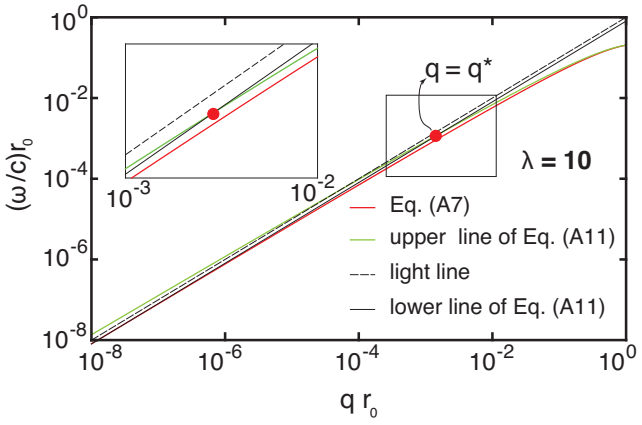


FIG. 4. 1D plasma dispersion relation, $\omega_p^{1D}(q)$. In contrast to ω_p^{2D}, ω_p^{1D} depends sensitively on the paramter $\lambda = (c/c^*)^2$, where c^* depends on the materials. The red solid curve is given by Eq. (A7). It goes atop the green solid curve [upper line of Eq. (A11)] for $q > q^*$ but collapses to the solid black line [lower line of Eq. (A11)] for $q < q^*$. Here $q^* \sim \exp\left(-\sqrt{\lambda}\right)$ drastically relies on λ, which makes quantum quasi-1D electron gases essentially immune from retardation effects (REs).

behaves asymptotically as follows

$$\omega_p^{1D} \approx \begin{cases} c^*\, q\, \sqrt{K_0(r_0 q)}, & \text{if } q \gg q^*, \\ (2\lambda)^{-1/4}\, c\, q, & \text{if } q \ll q^*, \end{cases} \tag{A11}$$

which is confirmed in Fig. 4, where ω_p^{1D} is plotted versus q.

Now we discuss the value of q^* in a variety of quasi-1D electron gases. We first consider systems bearing quadratic energy-momentum relation for charge carriers, $\varepsilon(p) = \frac{p^2}{2m}$, for which $F = \frac{n_0 e^2}{m}$ the same as for 2D. Such systems include quantum wires that may be fabricated out of conventional semiconductor heterostructures[44], semiconducting carbon nanotubes[48] and semiconducting armchair GNRs (aGNRs).[49] To facilitate the analysis, let us write $n_0 = n_0^* \times 10^8 \mathrm{cm}^{-1}$ and $m = m^* \times 9.1 \times 10^{-31}\mathrm{Kg}$. Then we have

$$c^* \approx 2.3 \sqrt{\frac{n_0^*}{m^*}}\, 10^6 \mathrm{ms}^{-1}, \quad \lambda \approx 1.7 \times 10^4 \times \frac{m^*}{n_0^*}. \tag{A12}$$

Taking $r_0 \sim 10^{-8}\mathrm{m}$ as typically realized, we get

$$q^* \sim 10^8 \mathrm{m}^{-1} \times \exp\left(-92 \times \sqrt{\frac{m^*}{n_0^*}}\right). \tag{A13}$$

In AlGaAs/GaAs quantum wires, commonly $n_0^* \sim 10^{-3}$ and $m^* \sim 0.1$. Therefore, the as-estimated q^* is vanishingly small and the crossover never happens for such parameters. However, considering that q^* is extremely sensitive to $\frac{m^*}{n_0^*}$ due to the exponetial relation, it might not be completely out of question to attain the observation. Actually, by increasing n_0^* to 0.1 and simultanesouly diminishing m^* to 0.001, we can increase q^* to $10^5 \mathrm{m}^{-1}$, which corresponds to a length of 10μm that is incredibly smaller than typical value. Hitherto we have not been aware of any materials which meet the demand.

Next we look at systems with linear dispersion, $\varepsilon(p) = \hbar v_F p$. In this catagory one finds metallic aGNRs, 2D topological insulators[50] and perhaps the so-called Su-Schrieffer-Heeger chains (such as polyacetylene, when Peierls instability is weak or suppressed by e.g. doping).[51] Now we have $F = e^2 h^{-1} v_F$ (see Appendix). The corresponding c^* and λ are given by

$$c^* \approx 0.05 \times \sqrt{c\, v_F}, \quad \lambda \approx 430 \times \frac{c}{v_F}. \tag{A14}$$

Since these systems have relatively smaller lateral dimension, we may take $r_0 \sim 10^{-10}\mathrm{m}$. This gives

$$q^* \sim 10^{10} \mathrm{m}^{-1} \times \exp\left(-15 \times \sqrt{\frac{c}{v_F}}\right), \tag{A15}$$

which does not hinge on carrier concentration. The magnitude of v_F is primarily set by the electronic hopping energy $t \sim 1\mathrm{eV}$, the lattice constant $a \sim 10^{-10}\mathrm{m}$ and the Planck constant $\hbar$, namely $v_F \sim \frac{t\,a}{\hbar} \sim 10^5 \mathrm{ms}^{-1}$ by dimensional analysis. Thus, q^* is too small to be realized in these systems.

Finally it might be worthwhile to mention zigzag GNRs (zGNRs).[49] zGNRs feature a pair of partially flat subbands which touch at the boundaries of the first Brillouin zone. Thus, they are always metallic. For very narrow zGNRs with only these subbands partially filled, we find $F = e^2 h^{-1} v(p_F)$, where $v(p_F)$ denotes the Fermi velocity. Eqs. (A14) and (A15) remain valid. Now that $v(p_F)$ is generically smaller than that for e.g. armchair ribbons, we expect that the corresponding q^* must be far beyond experimental reach.

The above analysis shows that quasi-1D systems are not suitable for studying REs-driven crossover in plasma dispersion. Indeed, REs are generally negligible in the systems considered above.

* wakabayashi.katsunori@nims.go.jp

1 D. Pines, Rev. Mod. Phys. **28**, 184 (1956).
2 D. Bohm and E. Gross, Phys. Rev. **75**, 1851 (1949).
3 R. A. Ferrell, Phys. Rev. **111**, 1214 (1958).
4 F. Stern, Phys. Rev. Lett. **18**, 546 (1967).
5 C. C. Grimes and G. Adams, Phys. Rev. Lett. **36**, 145 (1976).
6 T. Ando, A. B. Fowler, and F. Stern, Rev. Mod. Phys. **54**, 437 (1982).
7 A. L. Fetter, Ann. Phys. **81**, 367 (1973).
8 K. S. Novoselov, A. K. Geim, S. V. Morozov, D. Jiang, Y. Zhang, S. V. Dubonos, I. V. Grigorieva, and A. A. Firsov, Science **306**, 666 (2004).

[9] A. K. Geim and K. S. Novoselov, Nat. Mater. **6**, 183 (2007).
[10] L. Fu, C. L. Kane, and E. J. Mele, Phys. Rev. Lett. **98**, 106803 (2007).
[11] H. J. Zhang, C.-X. Li, X.-L. Qi, X. Dai, Z. Fang, and S.-C. Zhang, Nat. Phys. **5**, 438 (2009).
[12] T. O. Wehling, A. M. Black-Schaffer, and A. V. Balatsky, Adv. Phys. **76**, 1 (2014).
[13] X.-L. Qi and S.-C. Zhang, Rev. Mod. Phys. **83**, 1057 (2011).
[14] M. Jablan, M. Soljacic, and H. Buljan, Proc. IEEE **101**, 1689 (2013); A. Politano and C. Chiarello, Nanoscale **6**, 10927 (2014); F. Abajo, ACS Photonics **1**, 135 (2014).
[15] G. C. Dyer, G. R. Aizin, S. Preu, N. Q. Vinh, S. J. Allen, J. L. Reno, and E. A. Shaner, Phys. Rev. Lett. **109**, 126803 (2012).
[16] L. Ju, B. Geng, J. Horng, C. Girit, M. Martin, Z. Hao, H. A. Bechtel, X. Liang, A. Zettl, Y. R. Shen, and F. Wang, Nat. Nanotechnology **6**, 630 (2011).
[17] J. Gómez Rivas, M. Kuttge, P. Haring Bolivar, H. Kurz, and J. A. Sánchez-Gil, Phys. Rev. Lett. **93**, 256804 (2004).
[18] G. Gómez-Santos and T. Stauber, EPL **99**, 27006 (2012).
[19] O. Vafek, Phys. Rev. Lett. **97**, 266406 (2006).
[20] L. D. Landau and E. M. Lifshitz, *The Classical Theory of Fields* (BH, 1975).
[21] V. Shikin, S. Nazin, D. Heitmann, and T. Demel, Phys. Rev. B **43**, 11903 (1991).
[22] The validity of RPA and hence that of the present approach has been demonstrated in all dimensions. See e.g. Q. P. Li, S. Das Sarma and R. Joynt, Phys. Rev. B 45, 13713 (1992); S. A. Mikhailov, Phys. Rev. Lett. 113, 027405 (2014).
[23] V. Ryzhii, A. Satou, and T. Otsuji, J. Appl. Phys. **101**, 024509 (2007).
[24] F. Evanglisti, J. Appl. Phys. **114**, 124506 (2013).
[25] N. W. Ashcroft and N. D. Mermin, *Solid State Physics* (Brooks/Cole, Cengage Learning, 1976).
[26] D. B. Mast, A. J. Dahm, and A. L. Fetter, Phys. Rev. Lett. **54**, 1706 (1985).
[27] D. K. Ferry, S. M. Goodnick, and J. Bird, *Transport in Nanostructures* (Cambridge University Press, UK, 2009).
[28] A. K. Geim and A. H. MacDonald, Physics Today **60**, 35 (2007).
[29] A. H. C. Neto, F. Guinea, N. M. R. Peres, K. S. Novoselov, and A. K. Geim, Rev. Mod. Phys. **81**, 109 (2009).
[30] V. P. Gusynin, S. G. Sharapov, and J. P. Carbotte, Phys. Rev. B **75**, 165407 (2007); M. I. Katsnelson, *Carbon in Two Dimensions* (Cambridge University Press, Cambridge, UK, 2012).
[31] L. O. Nyakiti, V. D. Wheeler, N. Y. Garces, R. L. Myers-Ward, C. R. Eddy, and D. K. Gaskill, MRS Bullet. **37**, 1149 (2012).
[32] Y. Zhang, L. Zhang, and C. Zhou, Accounts of Chemical Research **46**, 2329 (2012).
[33] Y. Xu, I. Mitokowski, C. Liu, J. Tian, H. Nam, N. Alidoust, J. Hu, C.-K. Shih, M. Z. Hasan, and Y. P. Chen, Nat. Phys. **10**, 956 (2014).
[34] D. Kim, S. Cho, N. P. Butch, P. Syers, K. Kirshenbaum, S. Adam, J. Paglione, and M. S. Fuhrer, Nat. Phys. **8**, 459 (2012).
[35] K. Hosono and K. Wakabayashi, Appl. Phys. Lett. **103**, 033102 (2013).
[36] W. Norimatsu and M. Kusunoki, Phys. Chem. Chem. Phys. **16**, 3501 (2014).
[37] A. Mishchenko, J. S. Tu, R. V. Gorbachev, J. R. Wallbank, M. T. Greenaway, V. E. Morozov, S. V. Morozov, M. J. Zhu, S. L. Wong, F. Withers, C. R. Woods, Y.-J. Kim, K. Watanabe, T. Taniguchi, E. E. Vdovin, O. Makarovsky, T. M. Fromhold, V. I. Fal'ko, A. K. Geim, L. Eaves, and K. S. Novoselov, Nat. Nanotechnology **9**, 808 (2014).
[38] Y. Liu and R. F. Willis, Phys. Rev. B **81**, 081406(R) (2010).
[39] M. J. Manfra, Annl. Rev. Condensed Matt. Phys. **5**, 347 (2014).
[40] M. A. Gluba, D. Amkreutz, G. V. Troppenz, J. Rappich, and N. H. Nickel, Appl. Phys. Lett. **103**, 073102 (2013).
[41] B. Sensale-Rodriguez, Appl. Phys. Lett. **103**, 123109 (2013).
[42] Q. Li and S. Das Sarma, Phys. Rev. B **87**, 085406 (2013).
[43] T. Demel, D. Heitmann, P. Grambow, and K. Ploog, Phys. Rev. Lett. **66**, 2657 (1991).
[44] A. R. Goñi, A. Pinczuk, J. S. Weiner, J. M. Calleja, B. S. Dennis, L. N. Pfeiffer, and K. W. West, Phys. Rev. Lett. **67**, 3298 (1991).
[45] G. R. Aizin, N. J. M. Horing, and L. G. Mourokh, Phys. Rev. B **65**, 241311 (2002).
[46] L. Wendler and V. G. Grigoryan, J. Phys.: Condens. Matter **11**, 4199 (1999).
[47] T. Giamarch, *Quantum Physics in one dimension* (Oxford University Press, Oxford, UK, 2004) . Another way to think of this is to replace $\delta^2(\vec{r})$ in Eq. (A1) by a less intensive distribution such as a gaussian $g(r)$ with width variation $\sim r_0$. Then Eq. (A3) becomes $\psi_{q\omega}(\vec{r}) = 2s_{q\omega}\int d\vec{r}' K_0(\kappa|\vec{r}-\vec{r}'|)g(r')$. Then the limit $r \to 0$ becomes regular.
[48] R. Saito, G. Dresselhaus, and M. S. Dresselhaus, *Physical Properties of Carbon Nanotubes* (Imperial college Press, London, UK, 1998).
[49] K. Wakabayashi, K. Sasaki, T. Nakanish, and T. Enoki, Sci. Technol. Adv. Mater. **11**, 054504 (2010).
[50] C. L. Kane and E. J. Mele, Phys. Rev. Lett. **95**, 146802 (2005); B. A. Bernevig, T. L. Hughes, and S. C. Zhang, Science **314**, 1757 (2006).
[51] A. J. Heeger, S. Kivelson, J. R. Schrieffer, and W.-P. Su, Rev. Mod. Phys. **60**, 781 (1988).